Proceedings of the 21st ICSMGE, Vienna, Austria, 14 – 19 June 2026. Pistrol, Adam & Schweiger (eds.)
Published by: ÖGG, Austrian Society for Geomechanics, Salzburg, Austria, ISBN 978-3-9503898-4-5
https://doi.org/10.53243/ICSMGE2026-1480

3D characterization of internal deformation in drying fine sediments using X-ray tomography and micron-sized tracking markers

Ludi Li, Shuoshuo Xu, **Budi Zhao**
School of Civil Engineering, University College Dublin, Ireland, budi.zhao@ucd.ie

ABSTRACT: Drying-wetting cycles, intensified by climate change, alter the hydro-mechanical behavior of fine-grained soils, promoting desiccation cracks that compromise engineered structures. X-ray computed tomography (CT) with embedded micron-sized tracking markers enables non-destructive deformation tracking, yet the particle tracking method (PTM) faces challenges under large, complex deformations when many particles have similar morphology. This study proposes a hybrid PTM combining Local Relative Positioning (LRP) with an Artificial Neural Network (ANN) to enhance tracking robustness. LRP establishes local features of particles based on nearest neighbors, generating displacement fields used to train a Random Forest displacement-trend model. The ANN then integrates predicted trends with morphology-location discrepancies to link particles across scans. The method is demonstrated on drying bentonite pastes with micron-sized glass bubbles, imaged by high-resolution CT. Compared to ANN alone, the hybrid method captures more complete displacement and volumetric strain fields, particularly near the surface with large deformation, while reducing noise. Tracking accuracy improves from 78% (ANN) to 98% (hybrid). The results highlight the method's potential for precise and efficient deformation characterization in fine-grained soils under complex strain conditions.

KEYWORDS: Artificial Neural Network, desiccation crack, internal deformation, particle tracking, X-ray tomography.

1 INTRODUCTION

Climate change is increasing the frequency and severity of drying-wetting cycles, altering the mechanical and hydraulic properties of fine-grained soils relevant to engineered slopes and clay liners (Tang et al., 2018). During drying, shrinkage in fine sediments is driven by the development of matric suction, while deformation is typically constrained by substrate friction (Groisman and Kaplan, 1994; Peron et al., 2009). Surface flaws further promote non-uniform deformation and facilitate the initiation of desiccation cracks (Weinberger, 1999; Shin and Santamarina, 2011).

X-ray computed tomography (CT) has emerged as a powerful non-destructive tool for visualizing internal deformation in drying fine sediments (Julina and Thyagaraj, 2019; Tang et al., 2019; Zhao and Santamarina, 2020). However, the direct CT imaging of micron- to submicron-scale clay particles remains challenging. One solution is to embed tracer particles, such as tens-of-micron-sized particles, into the soil to enable deformation tracking (Ibeh et al., 2021). Xu et al. (2023) used an artificial neural network (ANN) algorithm to track embedded air bubbles in drying kaolinite, linking markers based on location and morphology. However, the particle tracking method (PTM) that rely on morphology becomes less effective when tracking with large numbers of particles with similar shapes, particularly under large and complex deformations.

Another PTM links particles based on relative location rather than shape (Patel et al., 2018). For example, Yang et al. (2022) developed the ScalE and Rotation Invariant Augmented Lagrangian Particle Tracking method (SerialTrack), which tracks particles based on their relative position to nearest , reducing the dependence on morphological data. This reduces the reliance on the accuracy of morphological data. Despite the wide uses in fluid mechanics, its applicability for soil deformation characterization has not been assessed.

In this study, we propose a hybrid particle tracking method that combines local relative positioning (LRP) with ANN to improve the robustness and efficiency of tracking deformation in fine sediments. The method is demonstrated on drying bentonite pastes containing embedded micron-sized glass bubbles. LRP first establishes a local coordinate system to track particles by minimizing differences in local positional similarity across images. A subset of the LRP results is then used to train a Random Forest (RF) model to predict the displacement trend. Finally, the ANN model incorporates these predicted trends, along with discrepancies in particle locations and morphology, to achieve accurate linkage across images.

2 EXPERIMENTAL SET-UP AND IMAGE PROCESSING

2.1 *Experimental set-up*

Bentonite powder with high liquid limit (*LL*=375%) was thoroughly mixed with 1.67% glass bubbles (40-80 μm in diameter, Gurit A230) by mass. The mixture was hydrated to near liquid limit and injected into an acrylic cylinder (8 mm diameter, 10 mm height). The embedded glass bubbles constituted a volume ratio of 0.67% within the bentonite paste, which was expected to have minimal impact on soil shrinkage and desiccation crack formation. To enhance sidewall adhesion, the inner surface of the container was first roughened using 400CW sandpaper and then coated with polyvinyl alcohol (PVA) to make it hydrophilic (Trantidou et al., 2017).

2.2 *Drying and X-ray CT scan process*

The sample was dried at 23°C and 50% relative humidity in a climate chamber (Memmert ICH260), with two CT scans collected during the drying process. Scan-1 was performed immediately after sample preparation. Scan-2 was performed after 120 min of drying, with a total water content reduction of 60%. The average water content of each sample before and after scanning was determined by a precision scale. To minimize evaporation and maintain consistent average water content during each scan, the sample container was wrapped in plastic film and subsequently scanned using a high-resolution X-ray scanner (Phoenix Nanotom M, GE). The reconstructed X-ray CT images had a spatial resolution of 5.56 μm, approximately 10% of the mean glass bubble diameter.

2.3 *Image processing*

Figure 2 shows the vertical grey-scale slices of the X-ray CT images for Scan-1 and Scan-2. Between Scan-1 and Scan-2, the sample experienced vertical shrinkage, particularly at the sample surface centre, along with the enlargement of surface flaws. A noticeable contrast was evident among the glass bubbles (air), bentonite, and acrylic container. To minimize image noise, we applied a median filter of size 3×3×3 voxels twice. Then, glass bubbles were separated from both the

bentonite and the container with the threshold determined from Otsu's method (Otsu, 1979).

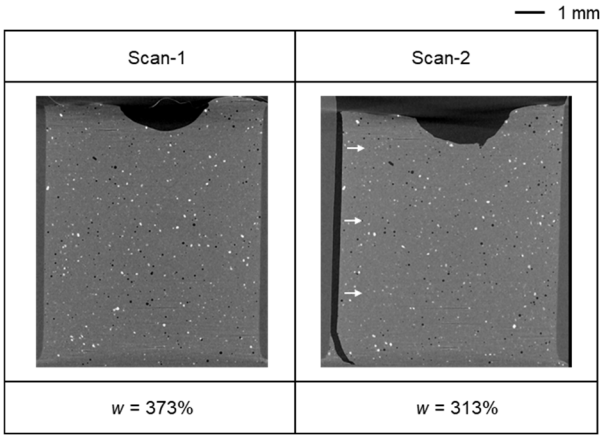

Figure 1. Vertical grey-scale images of the sample at the initial state (Scan-1), and after 120 min drying (Scan-2) with the representative water content.

The three-dimensional morphology and location of individual glass bubbles were obtained. The location data of each glass bubble are defined by the x, y, and z coordinates of its centroid. The morphology was quantified for both particle size and particle shape. Particle size parameters include volume (V) and surface area (SA), and particle shape parameters are sphericity (SP), aspect ratio (AR). More details of image processing and shape analysis were described in Zhao and Wang (2016).

A unified coordinate system was established based on six reference bubbles near the container base. Centroid coordinates of all bubbles in both scans were adjusted to this system to ensure consistency across datasets.

3 HYBRID LRP-ANN PARTICLE TRACKING METHOD

In this study, we adopted a hybrid particle tracking method that combines local relative positioning (LRP) with an ANN algorithm. The overall workflow of the hybrid method is illustrated in Figure 2. The LRP method is employed to obtain the overall displacement field (Yang et al., 2022), which is then used to train a displacement trend model using the Random Forest (RF) algorithm. Subsequently, the ANN, based on this displacement trend, is utilized to track particles across sequential scans by minimizing discrepancies in particle location and morphology, thereby identifying the most similar particle pairs (Xu et al., 2023).

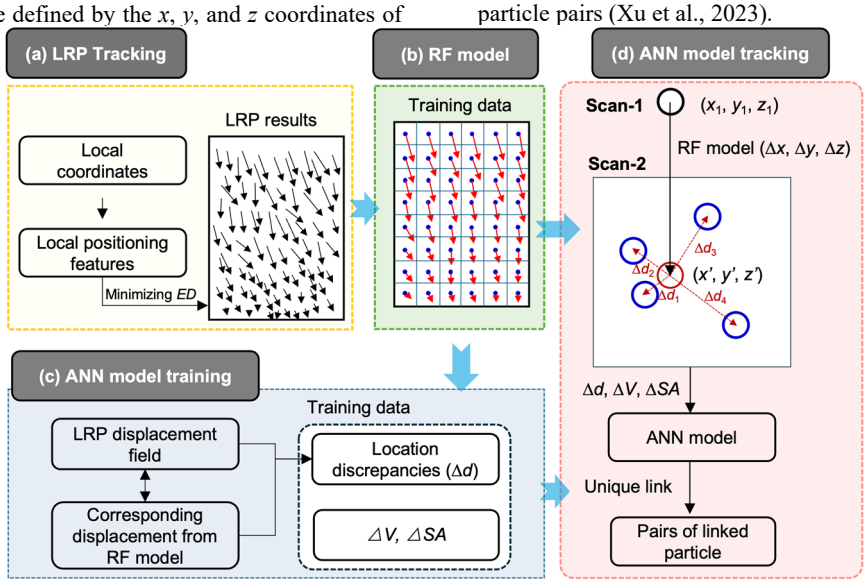

Figure 2. Flowchart of the hybrid particle tracking method with three main steps: (a) Local Relative Positioning (LRP) particle tracking; (b) displacement trend prediction with Random Forest (RF) model; (c & d) training and tracking with displacement-enhanced Artificial Neural Network (ANN) method.

The LRP process is shown in Figure 2a. To characterize the local geometry, each glass bubble was associated with a local coordinate system constructed using its k nearest neighbors. Based on this coordinate system, we defined a radial coordinate system with radial distance (r), polar angle (θ), and azimuthal angle (φ), allowing the k nearest neighbors of each particle to be described by feature vectors in this local coordinate system:

$$\boldsymbol{f_{i,j}} = \left(\widetilde{r_{i,j}}, \theta_{i,j}, \varphi_{i,j}\right) \quad (\text{for } j = 1,\ldots,k) \tag{1}$$

where i represents the i-th target particle in the scan, and j represents the j-th neighbor of the target particle; $\widetilde{r_{i,j}}$ represents the normalized radial distance, calculated as $\widetilde{r_{i,j}} = \frac{r_j}{r_{i,1}}$, where $r_{i,j}$ is the radial distance of the j-th neighbor particle and $r_{i,1}$ is the radial distance of the closest neighbor particle; $\theta_{i,j}$ and $\varphi_{i,j}$ represent the polar angle and azimuthal angle of particle j within the coordinate system, respectively. Then, a target particle i with its k nearest neighbors, can be represented by the local coordinate feature matrix as:

$$\boldsymbol{F_i} = \left[\boldsymbol{f_{i,1}}; \boldsymbol{f_{i,2}}; \cdots; \boldsymbol{f_{i,k}}\right] \tag{2}$$

For the first scan, a feature matrix $\boldsymbol{F_{1,i}}$ (where i represents the i-th target particle in the first scan) is constructed for each particle using its k nearest neighbors. Similarly, $\boldsymbol{F_{2,m}}$ represents the feature matrix of the m-th target particle in the second scan. To compare these two particles in sequential scans, a Euclidean distance (ED) was calculated using local feature matrices:

$$ED = \sqrt{\sum_{j=1}^{k}\left[\left(\widetilde{r_{i,j}} - \widetilde{r_{m,j}}\right)^2 + \left(\theta_{i,j} - \theta_{m,j}\right)^2 + \left(\varphi_{i,j} - \varphi_{m,j}\right)^2\right]} \tag{3}$$

where i and m represent the i-th particle in the first scan and the m-th particle in the second scan, respectively. Then, particles were matched iteratively by selecting the pair with the smallest distance, ensuring unique linking.

Second, LRP results were used to establish a displacement trend model using the Random Forest algorithm (Figure 2b). Displacements were first averaged within uniform

51-pixel cubes (approximately three times the mean bubble distance) to reduce noise and spatial irregularities. The RF model used the (x, y, z) coordinates of each cubic center point to learn the relationship between location and displacement. Once trained, the model outputs predicted displacements (Δx, Δy, Δz) from a given initial location.

Finally, we employed an artificial neural network (ANN) that identifies similar glass bubbles across scans by minimizing discrepancies in location and morphology (Figure 2c and Figure 2d). First, the RF model predicts displacement (Δx, Δy, Δz) based on the Scan-1 particle location (x_1, y_1, z_1), providing the predicted position (x', y', z') = ($x_1+\Delta x$, $y_1+\Delta y$, $z_1+\Delta z$). The location discrepancies between the predicted location and the location of candidate particles (x_2, y_2, z_2) within Scan-2 were served as ANN input parameters: $\Delta d_x = |x_2 - x'|$, $\Delta d_y = |y_2 - y'|$ and $\Delta d_z = |z_2 - z'|$. Also, particle size discrepancies of volume (ΔV) and surface area (ΔSA) were included as ANN inputs, combined with location discrepancies.

For improved tracking accuracy, a cubic search region centered at the predicted location (with a length of 34 pixels, around twice the mean glass bubble distance) is defined during the particle tracking process. Each particle in Scan-1 was compared with all candidates within the search region in Scan-2 to generate the correlation factors using the ANN model. A unique-linking algorithm was then applied, retaining only the matched pairs with the highest correlation factors. To train the ANN model, we selected a uniformly distributed subset of the filtered LRP results, comprising approximately 1% of the total glass bubbles, thereby avoiding the time-consuming manual linking of particles for ANN training.

4 RESULTS

4.1 *Displacement fields*

Figure 3 shows the vertical and horizontal displacement fields for Scan 1-2 obtained by the ANN method (following Xu et al., 2023) and the hybrid method proposed in this study. The displacement on the vertical plane is dominated by vertical shrinkage, whereas on the right sidewall the displacement magnitude is much smaller due to sidewall constraints. (Figure 3a and b). This reduction is less evident near the left sidewall because of the nearby crack (shown in Figure 1). The horizontal displacement field between Scan 1-2 is dominated by the crack formation near the left sidewall and shows significant horizontal displacement to the right (Figure 3c and d). A more detailed analysis of the displacement fields obtained by each method is presented below.

As shown in Figure 3a and 3c, ANN fails to capture the large, non-uniform deformation in certain regions, as indicated by the blue dashed lines. The tracking accuracy, calculated by comparing against manually linked partial results taken as the ground truth, is only 78%, as the ANN method struggles with large and complex deformation in the sample. This is due to the inconsistent location information across regions with varying deformation, and the ANN's heavy reliance on the morphological similarity of embedded tracking markers. As a result, the ANN fails to effectively capture displacement patterns within large and complex deformation regions.

On the other hand, the hybrid method captures a large, non-uniform deformation pattern in the crack formation region with negligible noise, highlighting the effects of crack formation and sidewall constraints on the sample's non-uniform deformation (Figure 3b and 3d). Overall, this hybrid approach produces a complete and smoother deformation pattern with reduced noise compared to the ANN results with a tracking accuracy of 98%.

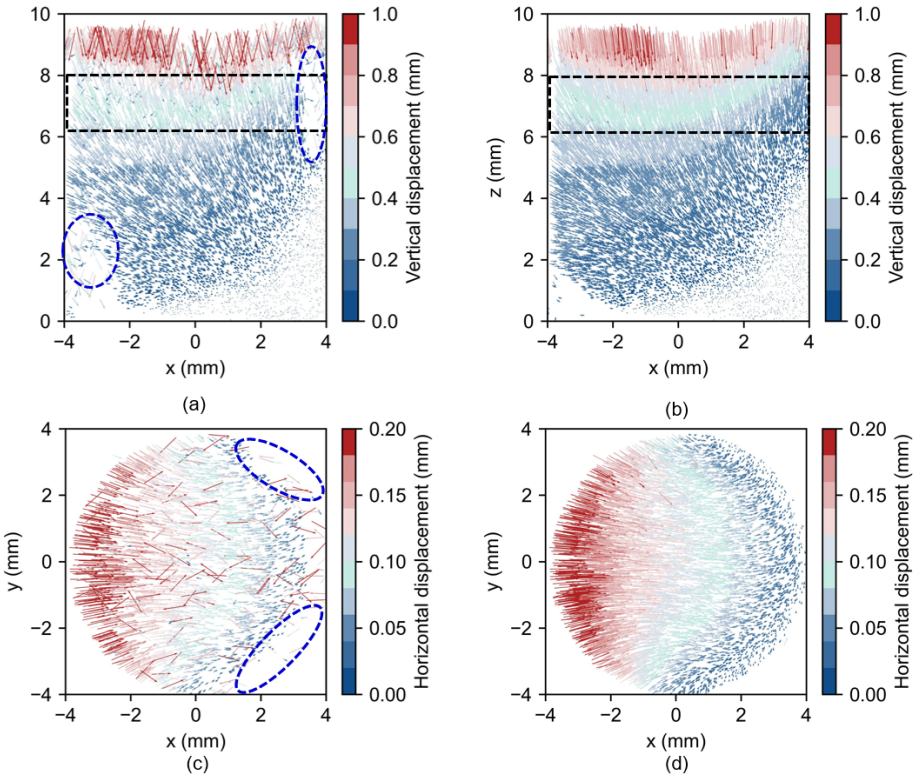

Figure 3. Vertical and horizontal displacement fields for Scan 1-2 using two methods: (a) vertical displacement fields (y = -1.0mm~1.0mm) using the ANN method; (b) vertical displacement fields (y = -1.0mm~1.0mm) using the hybrid method; (c) horizontal displacement fields using the ANN method; (d) horizontal displacement fields using the hybrid method. Note: The black dashed boxes indicate the corresponding depth of horizontal displacement field.

4.2 *Strain fields*

Based on the displacement fields, the volumetric strain (Figure 4) for Scans 1-2 of the middle plane was derived from both the ANN and hybrid methods. To reduce noise, average displacement was assigned within cubic regions of 52 pixels based on tracking results. The center points along with location and displacement were then used to define tetrahedral elements for computing the 3D strain fields, following Xu et al., (2023).

The sample exhibits a reduction in shrinkage from sample surface, with volumetric strain decreasing from nearly 20% at the surface to ~4% near the right bottom corner. This behavior is governed by the combined effects of higher moisture loss at the evaporation surface, constraint along the right sidewall, and crack formation on the left side. Near the surface, the lower region of the surface flaw exhibits smaller volumetric strain, ranging from 6.5% to 4%, whereas a much larger volumetric strain of around 20% develops near the sidewalls, due to the irregular geometry of the sample surface. The ANN result captures a volumetric strain pattern well in the lower region (z = 0-5 mm), where deformation is relatively small. However, the upper region exhibits substantial noise (Figure 4a). In contrast, the hybrid method captures a more complete volumetric strain field across the sample and achieves higher accuracy near the surface where large deformation occurs, while maintaining only minor noise (Figure 4b).

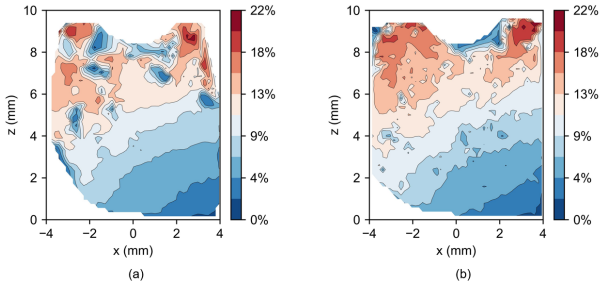

Figure 4. Distribution of volumetric strain ε_v at the vertical plane near the middle of sample for Scan 1-2 using (a) ANN method and (b) the hybrid method.

5 CONCLUSIONS

This study introduces a hybrid approach that integrates the Local Relative Positioning (LRP) method and an Artificial Neural Network (ANN) for particle tracking and characterizes the internal deformation of the drying fine sediment. Micron-sized glass bubbles were embedded in saturated bentonite pastes as tracking markers, and two CT scans were performed during the drying process to capture internal deformation before and after desiccation crack formation.

Image processing techniques were applied to extract the location and morphological information of the glass bubbles. The LRP method is employed to obtain the overall displacement field, which is then used to train a displacement trend model using the Random Forest (RF) method. Subsequently, the ANN based on this displacement trend is utilized to track particles across sequential scans by minimizing discrepancies in particle location and morphology, thereby identifying the most similar particle pairs.

The hybrid method successfully incorporates the particle displacement trend into the ANN model, combining the discrepancies of locations and morphology with surrounding particles, identifying the most similar glass bubble pairs with the highest correlation factors. The hybrid method successfully captures both large non-uniform and small deformation regions while maintaining smoother overall displacement and strain fields with a high tracking accuracy of 98%. In contrast, the ANN alone yields lower tracking accuracy, with limited capability in capturing large and non-uniform deformation regions and significant noise in these areas.

These results highlight the advantages of the hybrid method: by utilizing LRP results to construct a displacement trend model, integrating displacement trends into the ANN model can accurately and efficiently identify the best match for glass bubbles with minimal discrepancies of location and morphology. The hybrid method also mitigates the ANN's reliance on manually linked datasets, which can negatively affect tracking accuracy.

6 REFERENCES

Groisman, A. and Kaplan, E., 1994. An Experimental Study of Cracking Induced by Desiccation. *Europhysics Letters (EPL)*, 25(6), pp.415–420. https://doi.org/10.1209/0295-5075/25/6/004.

Ibeh, C.U., Pedrotti, M., Tarantino, A. and Lunn, R.J., 2021. PLATYMATCH–A particle-matching algorithm for the analysis of platy particle kinematics using X-ray Computed Tomography. *Computers and Geotechnics*, 138, p.104367.

Julina, M. and Thyagaraj, T., 2019. Quantification of desiccation cracks using X-ray tomography for tracing shrinkage path of compacted expansive soil. *Acta Geotechnica*, 14(1), pp.35–56. https://doi.org/10.1007/s11440-018-0647-4.

Otsu, N., 1979. A threshold selection method from gray-level histograms. *IEEE transactions on systems, man, and cybernetics*, 9(1), pp.62–66.

Patel, M., Leggett, S.E., Landauer, A.K., Wong, I.Y. and Franck, C., 2018. Rapid, topology-based particle tracking for high-resolution measurements of large complex 3D motion fields. *Scientific reports*, 8(1), p.5581.

Peron, H., Hueckel, T., Laloui, L. and Hu, L., 2009. Fundamentals of desiccation cracking of fine-grained soils: experimental characterisation and mechanisms identification. *Canadian Geotechnical Journal*, 46(10), pp.1177–1201.

Shin, H. and Santamarina, J.C., 2011. Desiccation cracks in saturated fine-grained soils: particle-level phenomena and effective-stress analysis. *Géotechnique*, 61(11), pp.961–972. https://doi.org/10.1680/geot.8.P.012.

Tang, A.M., Hughes, P.N., Dijkstra, T.A., Askarinejad, A., Brenčič, M., Cui, Y.J., Diez, J., Firgi, T., Gajewska, B. and Gentile, F., 2018. Atmosphere–vegetation–soil interactions in a climate change context; impact of changing conditions on engineered transport infrastructure slopes in Europe. *Quarterly Journal of Engineering Geology and Hydrogeology*, 51(2), pp.156–168.

Tang, C.-S., Zhu, C., Leng, T., Shi, B., Cheng, Q. and Zeng, H., 2019. Three-dimensional characterization of desiccation cracking behavior of compacted clayey soil using X-ray computed tomography. *Engineering Geology*, 255, pp.1–10. https://doi.org/10.1016/j.enggeo.2019.04.014.

Trantidou, T., Elani, Y., Parsons, E. and Ces, O., 2017. Hydrophilic surface modification of PDMS for droplet microfluidics using a simple, quick, and robust method via PVA deposition. *Microsystems & nanoengineering*, 3(1), pp.1–9.

Weinberger, R., 1999. Initiation and growth of cracks during desiccation of stratified muddy sediments. *Journal of structural geology*, 21(4), pp.379–386.

Xu, S., Lai, J., O'Kelly, B.C. and Zhao, B., 2023. 3D deformation and strain fields in drying kaolinite obtained from tracking internal bubbles using X-ray CT and ANN. *Acta Geotechnica*. https://doi.org/10.1007/s11440-023-01948-8.

Yang, J., Yin, Y., Landauer, A.K., Buyukozturk, S., Zhang, J., Summey, L., McGhee, A., Fu, M.K., Dabiri, J.O. and Franck, C., 2022. SerialTrack: ScalE and rotation invariant augmented Lagrangian particle tracking. *SoftwareX*, 19, p.101204.

Zhao, B. and Carlos Santamarina, J., 2020. Desiccation crack formation beneath the surface. *Geotechnique*, 70(2), pp.181–186. https://doi.org/10.1680/jgeot.18.T.019.

Zhao, B. and Wang, J., 2016. 3D quantitative shape analysis on form, roundness, and compactness with μCT. *Powder Technology*, 291, pp.262–275. https://doi.org/10.1016/j.powtec.2015.12.029.